HHS Public Access

Author manuscript

FASEB J. Author manuscript; available in PMC 2022 January 01.

Published in final edited form as:

FASEB J. 2021 January ; 35(1): e21150. doi:10.1096/fj.202001080RR.

Mechanical loading stimulates bone angiogenesis through enhancing type H vessel formation and downregulating exosomal miR-214–3p from bone marrow-derived mesenchymal stem cells

Xuetong Wang[1,#], **Xinle Li**[1,2,#], **Jie Li**[1,#], **Lidong Zhai**[1], **Daquan Liu**[1,2], **Abdusami Abdurahman**[1], **Yifan Zhang**[1], **Hiroki Yokota**[3], **Ping Zhang**[1,2,3,4,*]

[1]Department of Anatomy and Histology, School of Basic Medical Sciences, Tianjin Medical University, Tianjin 300070, China

[2]Key Laboratory of Hormones and Development (Ministry of Health), Tianjin Key Laboratory of Metabolic Diseases, Tianjin Medical University, Tianjin 300070, China

[3]Department of Biomedical Engineering, Indiana University-Purdue University Indianapolis, IN 46202, USA

[4]Tianjin Key Laboratory of Spine and Spinal Cord, Tianjin Medical University, Tianjin 300052, China

Abstract

Exosomes are important transporters of miRNAs, which play varying roles in the healing of the bone fracture. Angiogenesis is one of such critical events in bone healing, and we previously reported the stimulatory effect of mechanical loading in vessel remodeling. Focusing on type H vessels and exosomal miR-214–3p, this study examined the mechanism of loading-driven angiogenesis. MiRNA sequencing and qRT-PCR revealed that miR-214–3p was increased in the exosomes of the bone-losing ovariectomized (OVX) mice, while it was significantly decreased by knee loading. Furthermore, compared to the OVX group, exosomes, derived from the loading group, promoted the angiogenesis of endothelial cells. In contrast, exosomes, which were transfected with miR-214–3p, decreased the angiogenic potential. Notably, knee loading significantly improved the microvascular volume, type H vessel formation, and bone mineral density and contents, as well as BV/TV, Tb.Th, Tb.N, and Tb.Sp. In cell cultures, the overexpression of miR-214–3p in endothelial cells reduced the tube formation and cell migration. Collectively, this study demonstrates that knee loading promotes angiogenesis by enhancing the formation of type H vessels and downregulating exosomal miR-214–3p.

[*]Corresponding Author: Ping Zhang, MD, Department of Anatomy and Histology, School of Basic Medical Sciences, Tianjin Medical University, 22 Qixiangtai Road, Phone: 86-22-83336818, Fax: 86-22-83336810, pizhang@tmu.edu.cn.

[#]These authors contributed equally to the study.

AUTHOR CONTRIBUTIONS

P. Zhang designed research; X. Wang, X. Li, J. Li, A. Abdurahman, Y. Zhang and P. Zhang conducted research; X. Wang, X. Li, L. Zhai, D. Liu, H. Yokota and P. Zhang analyzed the data; P. Zhang wrote the manuscript. P. Zhang approved the final manuscript as submitted. P. Zhang accepted responsibility for the integrity of data analysis.

CONFLICT OF INTEREST

The authors declare that they have no conflict of interest.

Keywords

Osteoporosis; MiRNA; Vessel remodeling; Type H vessels; Knee loading

INTRODUCTION

Osteoporosis is a skeletal disorder characterized by loss of bone mass, micro-architectural deterioration, and a decline in bone quality.[1] Ovariectomy (OVX) surgery is a procedure to induce postmenopausal osteoporosis in animals. Animal models of osteoporosis are useful to evaluate treatment strategies.[2,3] Bone is a richly vascularized connective tissue, in which the vasculature is the main source of oxygen, nutrients, hormones, neurotransmitters, and growth factors.[4] Bone repair and remodeling involves complex angiogenic and osteogenic interactions. It has been demonstrated that angiogenesis precedes osteogenesis, and inadequate blood flow is linked to age-related low bone mass disorders such as osteoporosis.[5] During bone modeling and remodeling, it is reported that type H vessels, highly expressed with CD31 (platelet and endothelial cell adhesion molecule 1, PECAM-1) and Endomucin (Emcn), are formed in the bone.[6,7] Dysfunctional bone angiogenesis, which disrupts intraosseous homeostasis, is closely linked to the pathological process of osteoporosis.[4] VEGF is one of the important regulatory factors that couple angiogenesis with bone reconstruction.

Skeletal loading activates bone homeostasis by promoting bone formation,[8] and many loading modalities including whole-body vibration,[9] axial loading,[10] and four-point bending[11] are reported beneficial. In blood flow, shear stress and strain in the vessels are the major biomechanical parameters.[12] Mechanical forces play a crucial role in vascular injury and repair, which can directly activate the mechanosensing molecules.[13] We have developed joint loading modalities,[14] in which dynamic lateral loads are applied to synovial joints such as the elbow,[15] knee,[16] and ankle.[17,18] It is considered that mechanical loading induces dynamic deformation in the epiphysis that drives the alteration in intramedullary pressure in the medullary cavity and interstitial fluid flow in the lacunocanalicular network.[14] We previously reported that knee loading stimulated wound healing in the femoral neck and tibia,[19,20] prevented cartilage degeneration,[21,22] and promoted vessel remodeling and bone healing in osteoporosis of the femoral head.[23] The question herein is whether loading can promote the formation of type H vessels, and whether the regulation of microRNA (miRNA) is involved in loading-driven vessel/bone remodeling.

As nanometer-scale particles, exosomes are one form of extracellular vesicles (EVs) together with microvesicles and apoptotic bodies.[24,25] Exosomes are small vesicles of endocytic origin and are suggested to act as an essential mediator in intercellular communications.[26] For instance, bone marrow-derived mesenchymal stem cells (BMMSCs) play a vital role in osteoblastic differentiation via a paracrine pathway,[27] and several studies have demonstrated the role of BMMSC-derived EVs in vessel remodeling and bone healing. *In vivo* experiments revealed that exosomes markedly stimulated bone regeneration and angiogenesis in critical-sized calvarial defects in ovariectomized rats.[28] Moreover, exosomes that were secreted by induced pluripotent stem (iPS) cell-derived mesenchymal stem cells

(MSCs) prevented osteonecrosis of the femoral head.[29] However, the mechanism by which EVs such as BMMSC-derived exosomes (BMMSC-Exos) participate in mechanotransduction of bone is unclear.

MiRNAs are evolutionally conserved, non-coding, small RNAs (~22 nucleotides).[30] They play a fundamental role in cell proliferation, differentiation, and apoptosis, and many of them are associated with diseases and pathophysiological states. In the skeleton, some miRNAs are shown to suppress the inhibition of bone cell differentiation.[31] Many lines of evidence also indicate that miRNAs are excreted not only into the local bone environment but also into the circulation, implicating a local and systemic role of miRNAs. It has been demonstrated that exosomes with miR-126, miR-210, miR-132, and miR-139 promote endothelial cell viability, proliferation, and tube formation.[24,25] Focusing on the linkage between angiogenesis and bone remodeling, this study aimed to evaluate the potential role of miRNA in response to skeletal loading.

After miRNA screening and sequencing, this study specifically focused on the role of miR-214–3p (miR-214) in BMMSC-Exos. The level of exosomal miR-214–3p was elevated in elderly patients with bone fractures, and this miRNA inhibits osteoblastogenesis and reduces bone formation in the aged osteoporotic mice.[30] Most recently, miR-214–3p was reported to delay the healing of osteoporotic fracture in rats by inhibiting a BMP/Smad signaling pathway.[32] Another study also showed that miR-214–3p delayed the fracture healing in mice by inhibiting a Wnt/β-catenin signaling pathway.[33] In addition, *in vivo* studies demonstrated the impaired growth of vessels in pre-miR-214–3p-EV- treated mice.[34] In vitro osteoblast activity and matrix mineralization were promoted by antagomir-214 and decreased by agomir-214, in which miR-214 directly targeted ATF4 and inhibited osteoblast activity.[35] These data suggest that miR-214–3p has a crucial role in suppressing the bone formation and that miR-214–3p inhibition in osteoblasts is potentially an anabolic strategy for ameliorating osteoporosis.[26]

Our hypothesis was that exosomal miRNAs, in particular, miR-214–3p plays a fundamental role in the progression of osteoporosis, and it participates in the load-driven responses in osteogenesis and angiogenesis. To test the hypothesis, we employed osteoporotic mice with and without knee loading. Exosomes were harvested from conditioned media derived from BMMSCs and conducted miRNA sequencing. Bone marrow-derived cells were isolated to examine the differentiation of endothelial progenitor cells (EPCs). After validating the effects of exosomes *in vitro*, the agomir and antagomir of miR-214–3p were transfected *in vitro* to test their role in angiogenesis. Immunofluorescence and ink perfusion were performed to evaluate angiogenesis including type H vessels. This study provided new evidence for loading-driven promotion of angiogenesis in bone, and suggested that regulating exosomal miRNA can be a novel option for the treatment of skeletal diseases such as osteoporosis.

MATERIALS AND METHODS

Animals and materials preparation

All experiments were carried out according to the National Institutes of Health Guide for Care and Use of Laboratory Animals, and were approved by the Ethics Committee of Tianjin Medical University. Female C57BL/6 mice (16 weeks old, Animal Center of Academy of Military Medical Sciences, China) were used. One hundred and fifty-nine mice were randomly divided into 3 groups: the sham control group (Sham, n = 49), the ovariectomized group (OVX, n = 49), and the loading-treated ovariectomized group (OVXL, n = 61). Four to five mice per cage were fed with mouse chow and water ad libitum. Mice were housed on a 12 h light-dark cycle at room temperature of 25°C under pathogen-free conditions.

Cytokines were purchased from PeproTech (Rocky Hills, NC, USA). Medium, fetal bovine serum (FBS), Lipofectamine 3000 Reagent, penicillin, streptomycin, and trypsin were purchased from Invitrogen (Carlsbad, CA, USA). Endothelial cell growth medium-2 (EGM-2) Bullet Kit was obtained from Lonza (Walkersville, MD, USA). Matrigel was purchased from Life Sciences (Tewksbury, MA, USA). A DAB substrate kit was purchased from ZSGB-BIO Corporation (Beijing, China). A primary antibody specific to vascular endothelial growth factor receptor 2 (VEGFR2) was purchased from Cell Signaling (Danvers, MA, USA), and the antibodies for VEGF and β-actin were purchased from Abcam (Cambridge, MA, USA). Other chemicals were purchased from Sigma (St. Louis, MO, USA) unless otherwise stated.

Ovariectomy

Ovariectomy was performed as previously described.[36] Briefly, the mouse was anesthetized with 1.5% isoflurane at a flow rate of 1.0 L/min. The mouse was placed in a prone position, and the dorsal area was shaved and sterilized with 70% alcohol solution. A midline dorsal skin incision was made using a scalpel, and the ovaries were excised with scissors. For sham OVX-operated mice, the same procedure was conducted without removing the ovaries. To alleviate the pain associated with surgery, the mouse was administered a dose of 0.05 mg/kg buprenorphine hydrochloride every 8 h for the first three postoperative days. After surgery, 1% pramoxine hydrochloride ointment was applied on the incision sites every day for the first three postoperative days.

Mechanical knee loading

Two weeks after ovariectomy, the OVX-loaded mice were subject to mechanical stimulation (Figure 1A). During mechanical loading, the mouse was mask-anesthetized using 1.5% isoflurane. A custom-made mechanical loader was employed to apply loads to the right knee in the lateral-medial direction. After finishing the right knee loading, the same loading procedure was conducted on the left knee.[16] The sham control and OVX groups received sham loading, in which mice were positioned on the loading table without receiving dynamic loading to the knee. In the current study, loads with 1 N and 5 Hz were given for 6 min/day for 14 consecutive days. The loading device was calibrated using a load cell (Model

LLB130, FUTEK Advanced Sensor Technology, Irvine, CA, USA) to determine the compressive force. After loading, the mouse was allowed normal cage activity.

Cell culture

After the animals were humanely sacrificed, bone marrow-derived cells were collected by flushing the femur and tibia with MEM Alpha basic (MEM-α) containing 2% FBS. Mononuclear cells were isolated by density-gradient centrifugation with Ficoll (Sigma, MO, USA) and cultured at a density of 1×10^7 cells in 25-mm^2 fibronectin-coated flasks (Corning, NY, USA).[36] To obtain BMMSCs, mononuclear cells were cultured in MesenCult basal medium with MesenCult™ supplement. BMMSCs were cultured in MEM-α supplemented with 100 U/mL penicillin, 100 μg/mL streptomycin, and 10% fetal bovine serum (FBS, Gibco, USA) in 25-mm^2 fibronectin-coated flasks.[37] EPCs culture medium (EGM-2; Lonza) was supplemented with 100 U/mL penicillin, 100 μg/mL streptomycin, and 20% fetal bovine serum.[36] Furthermore, human umbilical vein endothelial cells (HUVECs) were cultured in Dulbecco's Modified Eagle's Medium (DMEM) supplemented with 100 U/mL penicillin, 100 μg/mL streptomycin, and 10% FBS. And we replaced the exosome-free medium to extract exosomes of BMMSCs. The exosome-free medium supplemented with 100 U/mL penicillin, 100 μg/mL streptomycin and 10% exosome-free FBS (ultracentrifugation at 120,000 g, 4°C for 14 h).

Immunofluorescence analysis

EPC purity was assessed by analyzing the surface expression of CD34 (Novos, NBP1–44407) and VEGFR2 (CST, 9698S) through immunofluorescence. Induced EPCs (2×10^5) were seeded in 24-well plates for 24 h, then washed three times in pre-cooled PBS, fixed with 4% paraformaldehyde, and permeabilized with 0.5% Triton X-100. After blocking with 10% normal goat serum, cells were incubated overnight at 4°C with anti-CD34 antibodies (1:100) and VEGFR2 (1:200). Subsequently, the samples were incubated with secondary antibodies conjugated with fluorescence at room temperature for 1.5 h (avoiding light). The expression of CD34 and VEGF were determined by fluorescence microscope, in which the nuclei were counterstained with DAPI.[36]

Exosomal extraction

BMMSCs were grown to sub-confluency (approximately 80%) before replacing with the exosome-free medium. After being cultured for 48 h, the medium was collected and centrifuged to remove cell debris.[38] Exosome purification was performed as previously described.[39] Cell culture media were used for exosome isolation with Umibio® exosome isolation kits (Umibio, Cat. China) according to the manufacturer's instructions. In brief, an initial spin was performed at 3,000 g for 10 min for each sample to remove cells and debris, then the corresponding amounts of reagents were added proportional to the starting sample volume, according to the manufacturer's instructions. Mixtures were vortexed and incubated at 4°C for up to 2 h and then centrifuged at 10,000 g for 60 min to precipitate exosome pellets. Pellets were resuspended with PBS and purified with Exosome Purification Filter at 3,000 g for 10 min. The resuspension volume for exosome pellets was 200 μl for 20 ml starting volumes according to the manufacturer's instructions. All exosomes were stored at −80°C immediately after isolation until further analysis.

Exosome identification

50 μl exosome solutions were placed on a copper screen at room temperature for 1 min. A filter paper was then used to extract the superfluous liquid. Afterward, the exosomes were negatively stained using the 1% (w/v) sodium phosphotungstate solution at room temperature for 3 min, and aspirated the solution with filter paper. Then placed the copper mesh under a tungsten lamp for 10 min. Afterward, the images were captured under the transmission electron microscope (HT7700, HITACHI, Japan). Exosomes (4 μg) were dissolved in 1 ml PBS solution and vortexed for 1 min to maintain a uniform distribution of exosomes. The NanoSight nanoparticle tracking analyzer (Nanosight NS300) was used to determine the diameter and scale distribution of microvesicles. Western blot analysis was conducted to identify the surface markers of exosomes. The protein lysates were separated on 10% SDS-polyacrylamide gels at 80 V and electrophoretically transferred to a nitrocellulose membrane at 350 mA for 2 h. After blocking with 5% nonfat milk, mouse monoclonal antibodies against CD63 (1:2000), and TSG101 (1:1000) (UR52301, Umibio, Shanghai, China) were incubated with the membrane at 4 °C overnight, followed by a brief wash and incubation with secondary antibody for 1.5 h at room temperature. Enhanced chemiluminescence was used to assess protein levels. Image acquisition and analysis software (Bio-rad) was used to quantify band intensities.

Exosomes uptake by HUVECs

To determine exosomes uptake by HUVECs, exosomes were labeled with a green fluorescent dye (PKH67, Sigma, USA) according to the manufacturer's instructions and incubated avoiding light at room temperature for 10 min, and later incubated with HUVECs at 37°C for 4 h. These cells were subsequently washed with PBS and fixed in 4% paraformaldehyde (PFA) for 15 min. Fixed cells were washed with PBS three times, incubated with DAPI for 5 min at room temperature. Fluorescence microscopy was applied to detect the green signals in cells.[40]

Determination of appropriate concentration

HUVECs were seeded onto 12-well plates with different concentrations of exosomes (0, 25 and 50 μg/mL). After 48 h, we examined the levels of VEGF through Western blot in HUVECs and the significant differences were detected. Then we seeded HUVECs onto 96-well plates with 25 μg/mL, and absorbance at 570 nm was detected using a μQuant universal microplate spectrophotometer. It also has significant differences. Then we determined the 25 μg/mL concentration of exosomes for further experiments.[37]

Exosomal miRNA screening

For exosomal miRNA sequencing with bone marrow-derived MSCs, total RNA was isolated from exosomes with a miRNeasy Mini kit (cat. No. 217004, Qiagen, Hilden, Germany). The RNA's samples were sent to TianGen for high-throughput sequencing and data analysis.[41] Using the single-ended 50 bp sequencing mode of the Illumina HiSeq2500 sequencing platform (TIANGEN BIOTECH CO., LTD, Beijing, China) to finish the high-throughput sequencing of samples.

Bioinformatics analysis

MiRNA target prediction was performed by using four databases: miRDB, miRTarBase, targetscan 7.2, and miRWalk Targets, and only the target genes predicted by three of four tools were taken into account.[42] For functional analyses of potential miRNA targets, Gene Ontology (GO) term analysis was applied to organize genes into categories based on biological processes by ToppGene.

MiRNA mimics and miRNA inhibitor transfection

According to the instructions, BMMSCs and HUVECs at 70–90% confluency were cultured in medium without penicillin and streptomycin and transfected with 50 nM miRNAs using Lipofectamine 3000 in Opti-MEM (Invitrogen, Carlsbad, CA, USA), according to the manufacturer's procedures.[43] The synthetic miR-214–3p mimic (Agomir), miR-214–3p mimic control (Agomir-NC), miR-214–3p inhibitor (Antgomir), and inhibitor control (Antgomir-NC) were purchased from GenePharma (Suzhou Huihe Pharma Co., LTD, Suzhou, China). After transfection for 6 h, the culture medium of HUVECs was replaced with DMEM supplemented with 10% FBS, 100 U/mL penicillin, and 100 μg/mL streptomycin. The culture medium of BMMSCs was replaced with an exosome-free medium supplemented with 10% FBS, 100 U/mL penicillin, and 100 μg/mL streptomycin. 48 h after transfection, HUVECs became ready for the following experiments and exosome-free medium of BMMSCs was be collected for exosomes.[44]

Quantitative RT-PCR

The expression level of miR-214–3p and VEGF was validated by using a Quantitative RT-PCR (qRT-PCR) system (QuantStudio 3, ABI, USA). Total RNA was extracted from human umbilical vein endothelial cells (HUVECs) and EPCs using an EasyPure RNA Kit ER101 (Transgen, Beijing, China). Exosomal miRNA was extracted through an EasyPure miRNA Kit ER601 (Transgen, Beijing, China). Reverse-transcribed into complementary DNA (cDNA) by TransScript One-Step Gdna Removal and cDNA Synthesis SuperMix AT341, AT311 and AT351 (Transgen). Subsequently, the diluted cDNA was used as temples in qPCR using TransStart Top Green qPCR SuperMix (Transgen) and specific primers. MiR-214–3p primers and VEGF primers were designed and synthesized by Sangon Biotech (Shanghai, China), and their sequences were listed in Table 1. The qRT-PCR consisted of 40 cycles (94°C for 5 s, 60°C for 30 s) after an initial denaturing step (50°C for 2 min, 94°C for 30 s). The expression levels were normalized against an internal reference and measured by the comparative Ct (ΔΔCt) method.[43]

In vitro tube formation assay

Prior to the assays for tube formation, cell migration, and wound healing, endothelial progenitor cells were induced from bone marrow-derived cells using the medium (EGM-2; Lonza), which was supplemented with 100 U/mL penicillin, 100 μg/mL streptomycin, and 20% fetal bovine serum. Immunostaining with antibodies specific to CD34 and VEGFR2 was conducted to confirm that the cultured cells were EPCs.[36] An in vitro Matrigel tube formation assay was performed to determine the angiogenic activity of EPCs as described previously.[36] The 24-well plates were coated with Matrigel and pre-incubated at 37°C in 1 h

for the tube formation assay. EPCs (2.5×10^5 cells) were incubated on the 24-well plates in 20% EGM2 for 10 h and cumulative tube lengths were counted. Furthermore, HUVECs (2.5×10^5 cells) were transfected with agomir-214–3p or antgomir-214–3p lentivirus and then seeded in Matrigel™ (BD Biosciences, USA) coated 24-well plates. The cells were cultured in 10% DMEM at 37°C with 5% CO_2 for 10 h. For the exosome's experiment, 2×10^4 HUVECs per well were seeded and cultured with 25 ug/mL exosomes for 16 h at 37°C.[37] Images were captured and the total number of tubes, which represented the degree of angiogenesis in vitro, was determined in four random fields (100 × magnification) per well.

Cell migration assay

A transwell chamber was used (8 μm, 24-well plate) for the migration assay.[36] EPCs were cultured in 25-mm^2 fibronectin-coated flasks with selective 20% FBS EGM-2 growth medium. Furthermore, HUVECs were cultivated in 10% FBS DMEM and infected with agomir-214–3p or antgomir-214–3p for 48 h. EPCs (2×10^4 cells/well) were suspended in serum-free medium in the upper chambers with the bottom chamber containing EGM-2 and 20% FBS. HUVECs (2×10^4 cells/well) were suspended in serum-free medium in the upper chambers with the bottom chamber that contained DMEM with 10% FBS. For the exosome's experiment, HUVECs (2×10^4 cells/well) were suspended in serum-free medium with 25 ug/mL exosomes in the upper chamber, the bottom chamber that contained DMEM with 10% FBS.[43] The number of cells that migrated to the lower surface in 12 h was counted using crystal violet staining.

Wound-healing assay

A wound-healing assay was performed for EPCs and HUVECs, using the procedure previously described.[45] Briefly, induced EPCs or HUVECs (2×10^6 cells) that were infected with agomir-214–3p or antgomir-214–3p were seeded in a six-well plate and grown to nearly 100% confluency. A linear scratch was then made with a 200-μl pipette tip. After being washed with PBS twice, replaced with the new medium. For the exosome's experiment, HUVECs (2×10^6 cells) were seeded. On reaching confluence, the sterile tip of a micropipette was used to make scratch wounds across each well. Each well was washed two times with PBS, and the basal medium was added containing exosomes at 25 ug/mL final concentration. Images for 3 fields of view per scratch were taken at 0 h, 24 h.[37] Images were taken at 0 h and 24 h at 100 × magnification, and the wound size was measured in three wells per group.

Cell viability assay

An MTT assay was used to evaluate cell viability as previously described.[46] Endothelial progenitor cells were cultured in 25-mm^2 fibronectin-coated flasks with selective EGM-2 growth medium. HUVECs were cultivated in 10% FBS DMEM and infected with agomir-214–3p or antgomir-214–3p for 48 h. Cells were seeded in 96-well plates at a density of 1×10^4 cells/well. After 48 h, the absorbance at 570 nm was detected using a μQuant universal microplate spectrophotometer (Bio-Tek, Winooski, USA).

Western blot analysis

Femurs or HUVECs were lysed in a RIPA lysis buffer to isolate proteins. Primary antibodies specific to VEGF, and β-actin were employed. Signals were detected with enhanced chemiluminescence. Signal intensities were quantified using the software Quantity One (Biorad, Hercules, CA, USA), following the manufacturer's instructions. The signal intensity of VEGF was normalized to β-actin intensity.[36]

Micro-computed tomography (μCT) and peripheral dual-energy X-ray absorptiometry (pDEXA) analysis

We used μCT to evaluate bone microstructure. Femora were analyzed by SkyScan 1276 micro-CT (Bruker, Kontich, Belgium). The scanner was set at 49 kV, a current of 200 μA, and a resolution of 8 μm per pixel.[3] The distal femur was selected to determine the trabecular bone volume fraction (BV/TV), trabecular thickness (Tb.Th), trabecular number (Tb.N), and trabecular separation (Tb.Sp).[47] Mice were imaged by peripheral dual-energy X-ray absorptiometry (pDEXA) in vivo.[36] The animal was anesthetized and placed in the prone position, and an image was acquired in ~5 min. BMD (g/cm^2) and BMC (g) of the whole body were determined without including the head. BMD/BMC of the hind limb (femur and tibia) were evaluated using mouse-specific software (version 1.47).

Bone immunofluorescence

To evaluate the extent of type H vessel formation, we conducted as previously described.[48] Briefly, freshly dissected bone tissues were immediately fixed in ice-cold 4% paraformaldehyde solution for 4 h, embedded the tissues in 8% gelatin (porcine) in the presence of 20% sucrose and 2% polyvinylpyrrolidone for 24 h. Embedded in OCT and cut into 25-μm-thick longitudinally oriented bone sections were stained with primary antibodies overnight at 4°C. And with the secondary antibodies at room temperature for 1 h while avoiding light. Sections incubated with secondary antibodies alone served as the negative controls. Nuclei were stained with DAPI. Images were acquired with an Olympus B53 fluorescence microscope (Olympus, Japan). Four randomly selected visual fields in the distal metaphysis of the femur were measured to calculate the percentages of type H vessels. Emcn, CD31 antibody, and all secondary antibodies were obtained from Abcam.

Blood perfusion assay

An ink perfusion assay using Chinese ink was performed to analyze bone angiogenesis.[36] The animals were anesthetized by an intraperitoneal injection of 10% chloral hydrate (3 ml/kg). A needle with a heparin-saline solution (25,000 units in 250 ml of 0.9% sodium chloride) was inserted into the left ventricle for liquid infusion. A 5% gelatin/ink solution was injected after clear liquid flowed from the right atrium. The femurs were harvested after the skin of animals became uniformly black. These tissues were fixed with 10% neutral buffered formalin for 2 days, and were decalcified in 14% EDTA for 2 weeks. The samples were cut into 15-μm thick slices. The vessel number per field and the ratio of vessel volume to total field area were calculated. For the histological assays, five fields per slice (100–400 ×) were randomly selected, and the structural and vascular parameters were determined using Cellsense Standard software (Olympus, Japan).

Bone immunohistochemistry

The femurs were fixed in 10% neutral buffered formalin for 2 days, and decalcified in 10% EDTA (pH 7.4) for 2 weeks. For immunohistochemistry, we used a DAB substrate kit (ZSGB-BIO, Beijing, China). The femurs were embedded in paraffin and coronally cut for 5-μm thick slices. One of every ten slices and totally five slices were chosen to quantify in each tissue. The sections of the distal femur were incubated with primary antibodies against VEGF. Quantitative analysis was conducted in a blinded fashion. To quantify VEGF expression, the ratio of VEGF positively stained area to total field area was calculated in 10 fields at 200 × magnification per section.[36]

Statistical analysis

The data were expressed as mean ± standard error of mean (SEM). For more than two-group comparisons, one-way ANOVA was conducted, followed by a post-hoc test using Fisher's protected least significant difference. For a two-group comparison, Student's t-test was conducted. All comparisons were two-tailed and statistical significance was assumed at $P < .05$. The asterisks (*, ** and ***) represent $P < .05$, $P < .01$ and $P < .001$, respectively.

RESULTS

The animal used for OVX and knee loading tolerated the procedures, and any abnormal behavior or diminished food intake was not observed. No obvious bruising or tissue damage was detected at the surgical and loading site.

Identification and internalization of exosomes

To characterize the exosomes that were isolated from BMMSCs, their morphological features, particle size, and surface markers were determined. We found disc-like structures with diameters in 40–160 nm by the electron microscope, which were consistent with the known exosomal structure (Figure 1B). Nanoparticle tracking analysis (NTA) was conducted to determine the concentration and particle-size distribution of the extracellular vesicles. The average particle size was 141.3 nm, indicating that these extracellular vesicles were in high quality (Figure 1C). Furthermore, the analyzed vesicles were positive for exosomal markers CD63, and TSG101 (Figure 1D). Finally, to determine whether the exosomes can be absorbed by the HUVECs, we used PKH67 green fluorescent dye to label the exosomes and observed their entry into the red fluorescent HUVECs (Figure 1E). These results indicated that BMMSCs released bona fide exosomes into the culture medium.

Comparison of total exosomal miRNAs expression

To visualize the expression pattern of exosomal miRNAs, a heat-map was constructed. The heat-map diagram showed a clear clustering of exosomal miRNAs in the sham group, OVX group, and OVX loading group. We selected 14 miRNAs, which presented significant changes after loading ($P < .05$), and the heat map was built based on the miRNA levels of the three groups. Compared to the sham group, 9 miRNAs (including miR-214–3p) were up-regulated, while 5 miRNAs were down-regulated in the OVX group. Notably, the OVX loading group showed the opposite trend (Figure 2A). We observed that miR-214–3p was up-regulated in exosomes (Figure 2B) and EPCs (Figure 2C) in the OVX group.

The biological functions of miR-214–3p

The identification of miRNAs, which were significantly linked to angiogenesis based on the predicted biological functions, highlighted miR-214–3p (Table S1, Figure 2B). The number of target genes of miR-214–3p was 699 (Figure 2D). The functions of these target genes were then determined using GO analysis, in which highlighted GO terms included tube development/morphogenesis, anatomical structure formation, cardiovascular/vasculature development, angiogenesis, and osteoclast differentiation (Figure 2E).

Characterization of mouse BM-derived EPCs

To characterize EPCs that were induced by bone marrow-derived cells, immunostaining analysis was conducted. We used antibodies specific to CD34 and VEGFR2 for detecting EPCs. The staining revealed that these EPCs expressed not only the hematopoietic stem cell marker, CD34, but also endothelial cell antigens such as VEGFR (Figure 3A). Of note, a combination of stem cell marker and endothelial cell marker was commonly used for identifying EPCs.

Promotion of endothelial tube formation, cells migration and wound healing by knee loading in vitro

To determine whether knee loading affected the angiogenesis of EPCs, tube formation, cell migration, and wound healing were assayed. Analysis of tube formation in bone marrow-derived EPCs showed that compared to the sham control, the samples derived from the OVX mice decreased tube lengths ($P < .05$). Compared to the samples derived from the OVX mice, however, the loading samples increased cumulative tube lengths ($P < .01$; Figure 3B, E). Similarly, compared to the sham control, the samples derived from the OVX mice decreased cell migration and wound healing (both $P < .001$). However, knee loading enhanced cell migration ($P < .01$; Figure 3C, F) and wound healing ($P < .001$; Figure 3D, G).

After re-plating, the third-passage cells appeared spindle-shaped and formed a homogenous monolayer and relative cell viability was evaluated by the MTT assay. Compared to the sham control, the samples derived from the OVX mice significantly decreased EPC viability in the MTT assay ($P < .001$). In contrast, knee loading enhanced it ($P < .001$; Figure 3H).

Exosomes effects of endothelial tube formation, cells migration, and wound healing

To determine whether knee loading affected angiogenesis via exosomal miR-214–3p, we added BMMSC-Exos to HUVECs and examined the effects of exosomes on tube formation, cell migration, and wound healing. Compared to the sham control, the BMMSC-Exos derived from the OVX mice decreased tube lengths and wound healing (both $P < .001$). However, knee loading increased cumulative tube lengths ($P < .001$; Figure 4A, D) and wound healing ($P < .001$; Figure 4C, F). Similarly, compared to the sham control, OVX treatment decreased cell migration ($P < .001$) and knee loading enhanced it ($P < .01$; Figure 4B, E). Compared to the sham control, OVX mice decreased HUVEC cell viability ($P < .05$), while knee loading enhanced it ($P < .001$; Figure 4G). We increased the level of exosomal miR-214–3p in the loading group with agomir-214–3p (L-agomir), and observed that the agomir significantly decreased tube formation ($P < .001$; Figure 4A, D), cell

migration ($P < .001$; Figure 4B, E) and wound healing ($P < .001$; Figure 4C, F). Furthermore, agomir-214–3p reduced cell viability ($P < .001$; Figure 4G).

MiR-214–3p regulates endothelial tube formation, cells migration and wound healing in HUVECs

We then tested whether miR-214–3p suppressed angiogenesis, tube formation, cell migration, and wound healing in HUVECs. Agomir-214–3p decreased tube formation ($P < .01$; Figure 5A, D), cell migration ($P < .001$; Figure 5B, E), and wound healing ($P < .05$; Figure 5C, F). Furthermore, agomir-214–3p reduced HUVEC cell viability ($P < .05$; Figure 5G). In contrast, antgomir-214–3p presented the responses opposite to agomir-214–3p ($P < .05$ in Figure 5H, K; $P < .001$ in Figure 5I, L; and $P < .05$ in Figure 5J, M). Furthermore, antgomir-214–3p enhanced HUVEC cell viability ($P < .05$; Figure 5N). Collectively, the result herein is consistent with the predicted inhibitory function of miR-214–3p.

MiR-214–3p-mediated promotion of bone angiogenesis by knee loading

To determine miR-214–3p-mediated effects of angiogenesis and the role of knee loading, we examined the level of VEGF in the femur (Figure 6A) and EPCs (Figure 6B). The expression of VEGF, which is one of the most important factors in angiogenesis, was decreased in OVX mice in the femur ($P < .01$) and EPCs ($P < .001$). However, compared to the OVX group, knee loading enhanced the level of VEGF in the femur ($P < .05$) and EPCs ($P < .01$).

To further explore the potential mechanism underlying the effect of miR-214–3p, we analyzed the protein level of VEGF in response to miR-214–3p overexpression or deletion. Agomir-214–3p decreased the level of VEGF in HUVECs ($P < .05$; Figure 6C), but antgomir-214–3p increased it ($P < .05$; Figure 6D).

Improvement of bone loss by knee loading in vivo

To test the effect of knee loading on bone loss, μCT and pDEXA imaging were conducted. Compared to the sham control, OVX mice decreased BV/TV ($P < .001$), Tb.N ($P < .001$), and Tb.Th ($P < .01$) in the distal femur, with an increase in Tb.Sp ($P < .001$). Two-week application of daily knee loading, however, elevated BV/TV ($P < .001$), Tb.N ($P < .001$), and Tb.Th ($P < .05$) with a decrease in Tb.Sp ($P < .001$; Figure 7A).

OVX mice also presented a reduction in BMD ($P < .001$) and BMC ($P < .01$) in the hind limb (femur and tibia) in pDEXA images, whereas the loaded OVX mice exhibited an increase in BMD ($P < .01$) and BMC ($P < .05$) (Figure 7B).

Promotion of angiogenesis by knee loading

To evaluate the effect of knee loading in bone angiogenesis, the expression of VEGF was determined in the distal femur by bone immunohistochemistry. VEGF was significantly decreased in OVX mice, based on the ratio of VEGF-stained area to the total field area in OVX mice ($P < .01$). However, knee loading increased the area of VEGF staining ($P < .05$; Figure 7C).

Increase of microvascular volume and type H vessels by knee loading in vivo

To test the effect of knee loading on angiogenesis, type H vessels were quantified by bone immunofluorescence and microvessels were detected in the ink perfusion assay. Compared to the sham group, the number and ratio of type H vessels were decreased at the meta-end of the femoral shaft in the OVX group ($P < .01$). However, knee loading suppressed the inhibitory effect of OVX ($P < .05$; Figure 7D). In addition, microvessels in the distal femur of OVX mice were determined using ink perfusion angiography. The OVX group showed a decrease in the vessel number ($P < .01$) and the ratio of the vascular area to the total area ($P < .01$), while knee loading increased them (both $P < .05$; Figure 7E).

DISCUSSION

The present study reveals that knee loading can protect from OVX-induced bone loss by promoting bone angiogenesis in the mouse model of postmenopausal osteoporosis. Knee loading stimulated the type H vessel formation and promoted angiogenesis by downregulating exosomal miR-214–3p (Figure 8). To identify exosomal miRNAs specifically involved in the progression of osteoporosis, miRNA screening and sequencing were conducted. It was revealed that miR-214–3p was increased in the exosomes of the OVX group, but it was markedly decreased by knee loading. Two-week application of daily knee loading suppressed OVX-induced bone loss and enhanced the formation of type H vessels. We also found that the tube formation, cell migration and wound healing of EPCs as well as the expression of VEGF were enhanced in the loading group. Compared to the OVX group, the exosomes in the loading group improved the tube formation, cell migration and wound healing of HUVECs. After increasing the expression of exosomal miR-214–3p in the loading group, the loading effect has reduced. Supplementing miR-214–3p inhibited tube formation, cell migration and wound healing, as well as expression of VEGF. However, the inactivation of miR-214–3p reversed the responses. Collectively, the result demonstrates that knee loading improves postmenopausal osteoporosis by enhancing type H vessel formation and downregulating exosomal miR-214–3p.

Osteoporosis is a disease characterized by deteriorated bone microstructure, loss in bone mineral density, and reduced bone quality, leading to lower bone strength and an increased risk of fracture. Reduction in mechanical loading accelerates the age-dependent bone loss, whereas increased loading via weight-bearing physical activity can increase bone strength by regaining bone mass and changing its macro- and micro-architecture.[49] Bone has the unique ability to modify its structure in response to skeletal loading.[8] Previous reports show that skeletal loading is a key regulator of bone metabolism, bone turnover, growth and mineralization.[10,11] Other stimulations such as whole-body vibration are reported to enhance bone formation and accelerate fracture healing.[9,50,51] Our previous works have shown that knee loading promotes bone formation and accelerates bone healing.[18,19,20] Thus, the current study extends the previous findings, which have demonstrated that knee loading is capable of increasing BMD and BMC in a mouse model of postmenopausal osteoporosis.

Mechanical forces such as shear stress and cyclic strain can regulate the adhesion, proliferation, migration, and differentiation of stem cells via serious signaling pathways. The enrichment and differentiation of stem cells play an important role in the angiogenesis and

maintenance of vascular homeostasis.[52] Exosomes and microvesicles are derived from MSCs, osteoblasts, osteoclasts and their precursors. As an important linker, they are shown to play pivotal roles in bone remodeling, including osteogenesis, osteoclastogenesis, and angiogenesis.[26] Especially, transplantation of BMMSC-Exos exerts a critical effect on the treatment of nonunion by promoting osteogenesis and angiogenesis.[53] Exosomal miRNAs have greatly influenced the regulation of bone formation and remodeling,[54] suggesting them as potential therapeutic targets. To confirm the function of miRNA in BMMSC-Exos, a deep understanding of the responses of mechanical stimulation and the underlying mechanisms involved in this process is essential for clinical translation. In the current study, we extracted BMMSC-Exos and miRNAs high-throughput screening and sequencing were conducted. qRT-PCR also confirmed that miR-214–3p in the OVX exosomes were reduced by knee loading. We harvested BMMSC-Exos which derived from over-expressed miR-214–3p BMMSCs and found it counteracted the pro-vascular regenerative functions of loading. These results indicated that knee loading played a therapeutic role by effectively suppressed BMMSC-Exos miR-214–3p in a mouse model of postmenopausal osteoporosis.

Bone vascularization is essential for many physiological processes, such as bone development and growth, and bone remodeling.[26] The secretion of VEGF is a step for the coupling of osteogenesis with angiogenesis. VEGF acts as a chemotactic molecule, attracting endothelial cells towards bone tissue and controlling the differentiation of osteoblasts and osteoclasts.[5] Our previous works demonstrated that osteonecrosis decreased the vessel volume, vessel number and expression of VEGF, but knee loading elevated them.[23] The current study also showed that knee loading enhanced tube formation, cell migration, and wound healing of EPCs, as well as the expression of VEGF. Supplementing miR-214–3p inhibited tube formation, cell migration and wound healing, and reduced the protein level of VEGF. Conversely, the inactivation of miR-214–3p reversed the responses. This result was consistent with previous reports that miR-214–3p negatively regulated angiogenic signaling via direct targeting of QKI and subsequent reduction of pro-angiogenic growth factor expression and release.[55] qRT-PCR showed that the trend of miR-214–3p level in EPCs was consistent with BMMSC-Exos, which corresponded with the results of EPCs experiments in vitro. It further verified our hypothesis that high expression of miR-214–3p inhibited angiogenesis. Therefore, EPCs, as a downstream of BMMSCs, was probably regulated by exosomal miR-214–3p derived from BMMSCs and affected its own expression of miR-214–3p. Meanwhile, the increase of type H vessels has a certain therapeutic effect on postmenopausal osteoporosis.[56] Notably, we observed that near the growth plate, the type H vessels were increased in the loading group, indicating the beneficial role of loading in vasculature growth. This study is the first to verify that mechanical stimulation has a positive effect on type H vessels. Previous research shows that the VEGF pathway controls the coupling of angiogenesis and osteogenesis by affecting the formation of type H vessels.[57] The results showed that the expression of VEGF, which is important for type H vessel formation, was regulated by miR-214–3p, and the promotion of type H vessel formation in response to mechanical loading was linked to exosomal miR-214–3p. Next, we will explore the mechanism of mechanical stress on type H vessels. Collectively, the results indicate that knee loading can promote vessel formation through enhancing type H vessel formation and downregulating miR-214–3p of BMMSC-Exos.

In summary, this study indicates that mechanical loading can be a new potential therapy for the treatment of postmenopausal osteoporosis by regulating not only osteogenesis but also the development of EPCs and angiogenesis. The action of mechanical loading is mediated by type H vessels and exosomal miR-214–3p, which may serve as a therapeutic target for skeletal diseases that may benefit from stimulated osteogenesis and angiogenesis.

Supplementary Material

Refer to Web version on PubMed Central for supplementary material.

ACKNOWLEDGMENTS

This work was supported by grants from the National Natural Science Foundation of China (81772405 and 81572100 to P. Zhang; 81601863 to X. Li; 31871212 to L. Zhai), Natural Science Foundation of Tianjin (18JCQNJC82200 to X. Li), and NIH (AR052144 to H. Yokota).

ABBREVIATIONS:

BMC	bone mineral content
BMD	bone mineral density
BMMSCs	bone marrow mesenchymal stem cells
BMMSC-Exos	BMMSC-derived exosomes
DMEM	Dulbecco’s Modified Eagle’s Medium
EDTA	ethylenediaminetetraacetic acid
EGM-2	Endothelial cell growth medium-2
EPC	endothelial progenitor cell
EVs	extracellular vesicles
FBS	fetal bovine serum
HUVECs	human umbilical vein endothelial cells
MEM-α	MEM Alpha basic
miRNAs	microRNAs
MSCs	mesenchymal stem cells
OVX	ovariectomized
pDEXA	peripheral dual-energy X-ray absorptiometry
PFA	paraformaldehyde
VEGF	vascular endothelial growth factor
VEGFR2	vascular endothelial growth factor receptor 2

REFERENCES

1. Compston JE, McClung MR, Leslie WD. Osteoporosis. Lancet. 2019;393:364–376. [PubMed: 30696576]
2. Huang L, Wang X, Cao H, et al. A bone-targeting delivery system carrying osteogenic phytomolecule icaritin prevents osteoporosis in mice. Biomaterials. 2018;182:58–71. [PubMed: 30107270]
3. Xie H, Cui Z, Wang L, et al. PDGF-BB secreted by preosteoclasts induces angiogenesis during coupling with osteogenesis. Nat Med. 2014;20:1270–1278. [PubMed: 25282358]
4. Filipowska J, Tomaszewski KA, Niedźwiedzki Ł, et al. The role of vasculature in bone development, regeneration and proper systemic functioning. Angiogenesis. 2017;20:291–302. [PubMed: 28194536]
5. Saran U, Gemini Piperni S, Chatterjee S. Role of angiogenesis in bone repair. Arch Biochem Biophys. 2014;561:109–117. [PubMed: 25034215]
6. Fu R, Lv WC, Xu Y, et al. Endothelial ZEB1 promotes angiogenesis-dependent bone formation and reverses osteoporosis. Nat Commun. 2020;11:460. [PubMed: 31974363]
7. Peng Y, Wu S, Li Y, et al. Type H blood vessels in bone modeling and remodeling. Theranostics. 2020;10:426–436. [PubMed: 31903130]
8. Wang C, Shan S, Wang C, et al. Mechanical stimulation promote the osteogenic differentiation of bone marrow stromal cells through epigenetic regulation of Sonic Hedgehog. Exp Cell Res. 2017;352:346–356. [PubMed: 28215635]
9. Jing D, Luo E, Cai J, et al. Mechanical vibration mitigates the decrease of bone quantity and bone quality of leptin receptor-deficient db/db mice by promoting bone formation and inhibiting bone resorption. J Bone Miner Res. 2016;31:1713–1724. [PubMed: 26990203]
10. Holguin N, Brodt MD, Silva MJ. Activation of Wnt signaling by mechanical loading is impaired in the bone of old mice. J Bone Miner Res. 2016;31:2215–2226. [PubMed: 27357062]
11. Yamasaki Y, Nagira K, Osaki M, et al. Effects of eldecalcitol on cortical bone response to mechanical loading in rats. BMC Musculoskelet Disord. 2015;16:158. [PubMed: 26123128]
12. Qi YX, Han Y, Jiang ZL. Mechanobiology and vascular remodeling: from membrane to nucleus. Adv Exp Med Biol. 2018;1097:69–82. [PubMed: 30315540]
13. Tian GE, Zhou JT, Liu XJ, et al. Mechanoresponse of stem cells for vascular repair. World J Stem Cells. 2019;11:1104–1114. [PubMed: 31875871]
14. Zhang P, Hamamura K, Yokota H, et al. Potential applications of pulsating joint loading in sports medicine. Exerc Sport Sci Rev. 2009;37:52–56. [PubMed: 19098525]
15. Zhang P, Yokota H. Elbow loading promotes longitudinal bone growth of the ulna and the humerus. J Bone Miner Metab. 2012;30:31–39. [PubMed: 21748461]
16. Zheng WW, Ding BB, Li XL, et al. Knee loading repairs osteoporotic osteoarthritis by relieving abnormal remodeling of subchondral bone via Wnt/β-catenin signaling. FASEB J. 2020;34:3399–3412. [PubMed: 31925860]
17. Yang S, Liu H, Zhu L, et al. Ankle loading ameliorates bone loss from breast cancer-associated bone metastasis. FASEB J. 2019;33:10742–10752. [PubMed: 31266364]
18. Zhang P, Turner CH, Yokota H. Joint loading-driven bone formation and signaling pathways predicted from genome-wide expression profiles. Bone. 2009;44:989–998. [PubMed: 19442616]
19. Zhang P, Turner CH, Yokota H. Knee loading stimulates healing of mouse bone wounds in a femur neck. Bone. 2011;49:867–872. [PubMed: 21723427]
20. Zhang P, Sun Q, Turner CH, et al. Knee loading accelerates bone healing in mice. J Bone Miner Res. 2007;22:1979–1987. [PubMed: 17696761]
21. Li X, Yang J, Liu D, et al. Knee loading inhibits osteoclast lineage in a mouse model of osteoarthritis. Sci Rep. 2016;6:24668. [PubMed: 27087498]
22. Zheng WW, Li XL, Liu DQ, et al. Mechanical loading mitigates osteoarthritis symptoms by regulating endoplasmic reticulum stress and autophagy. FASEB J. 2019;33:4077–4088. [PubMed: 30485126]

23. Liu DQ, Li XL, Li J, et al. Knee loading protects against osteonecrosis of the femoral head by enhancing vessel remodeling and bone healing. Bone. 2015;81:620–631. [PubMed: 26416150]
24. Liu M, Sun Y, Zhang Q. Emerging role of extracellular vesicles in bone remodeling. J Dent Res. 2018;97:859–868. [PubMed: 29566346]
25. Qin Y, Sun R, Wu C, et al. Exosome: a novel approach to stimulate bone regeneration through regulation of osteogenesis and angiogenesis. Int J Mol Sci. 2016;17:712.
26. Behera J, Tyagi N. Exosomes: mediators of bone diseases, protection, and therapeutics potential. Oncoscience. 2018;5:181–195. [PubMed: 30035185]
27. Santos TS, Abuna RP, Castro Raucci LM, et al. Mesenchymal stem cells repress osteoblast differentiation under osteogenic-inducing conditions. J Cell Biochem. 2015;116:2896–2902. [PubMed: 26013001]
28. Qi X, Zhang J, Yuan H, et al. Exosomes secreted by human-induced pluripotent stem cell-derived mesenchymal stem cells repair critical-sized bone defects through enhanced angiogenesis and osteogenesis in osteoporotic rats. Int J Biol Sci. 2016;12:836–849. [PubMed: 27313497]
29. Liu X, Li Q, Niu X, et al. Exosomes secreted from human-induced pluripotent stem cell-derived mesenchymal stem cells prevent osteonecrosis of the femoral head by promoting angiogenesis. Int J Biol Sci. 2017;13:232–244. [PubMed: 28255275]
30. Li D, Liu J, Guo B, et al. Osteoclast-derived exosomal miR-214–3p inhibits osteoblastic bone formation. Nat Commun. 2016;7:10872. [PubMed: 26947250]
31. Van der Eerden BC. MicroRNAs in the skeleton: cell-restricted or potent intercellular communicators? Arch Biochem Biophys. 2014;561:46–55. [PubMed: 24832391]
32. Zhou LG, Shi P, Sun YJ, et al. MiR-214–3p delays fracture healing in rats with osteoporotic fracture through inhibiting BMP/Smad signaling pathway. Eur Rev Med Pharmacol Sci. 2019;23:449–455. [PubMed: 30720150]
33. Teng JW, Ji PF, Zhao ZG. MiR-214–3p inhibits β-catenin signaling pathway leading to delayed fracture healing. Eur Rev Med Pharmacol Sci. 2018;22:17–24. [PubMed: 29364467]
34. Lombardo G, Gili M, Grange C, et al. IL-3R-alpha blockade inhibits tumor endothelial cell-derived extracellular vesicle (EV)-mediated vessel formation by targeting the β-catenin pathway. Oncogene. 2018;37:1175–1191. [PubMed: 29238040]
35. Wang X, Guo B, Li Q, et al. MiR-214 targets ATF4 to inhibit bone formation. Nat Med. 2013;19:93–100. [PubMed: 23223004]
36. Li X, Liu D, Li J, et al. Wnt3a involved in the mechanical loading on improvement of bone remodeling and angiogenesis in a postmenopausal osteoporosis mouse model. FASEB J. 2019;33:8913–8924. [PubMed: 31017804]
37. Ding J, Wang X, Chen B, et al. Exosomes derived from human bone marrow mesenchymal stem cells stimulated by deferoxamine accelerate cutaneous wound healing by promoting angiogenesis. Biomed Res Int. 2019;2019:9742765. [PubMed: 31192260]
38. Ma T, Chen Y, Chen Y, et al. MicroRNA-132, delivered by mesenchymal stem cell-derived exosomes, promote angiogenesis in myocardial infarction. Stem Cells Int. 2018;2018:3290372. [PubMed: 30271437]
39. Wang B, Wang X, Hou D, et al. Exosomes derived from acute myeloid leukemia cells promote chemoresistance by enhancing glycolysis-mediated vascular remodeling. J Cell Physiol. 2019;234:10602–10614. [PubMed: 30417360]
40. Huang JH, Xu Y, Yin XM, et al. Exosomes derived from miR-126-modified MSCs promote angiogenesis and neurogenesis and attenuate apoptosis after spinal cord injury in rats. Neuroscience. 2020;424:133–145. [PubMed: 31704348]
41. Fishman A, Light D, Lamm AT. QsRNA-seq: a method for high-throughput profiling and quantifying small RNAs. Genome Biol. 2018;19:113. [PubMed: 30107842]
42. Ren H, Yu X, Shen G, et al. MiRNA-seq analysis of human vertebrae provides insight into the mechanism underlying GIOP. Bone. 2019;120:371–386. [PubMed: 30503955]
43. Tian X, Yu C, Shi L, et al. MicroRNA-199a-5p aggravates primary hypertension by damaging vascular endothelial cells through inhibition of autophagy and promotion of apoptosis. Exp Ther Med. 2018;16:595–602. [PubMed: 30116316]

44. Shang S, Wang J, Chen S, et al. Exosomal miRNA-1231 derived from bone marrow mesenchymal stem cells inhibits the activity of pancreatic cancer. Cancer Med. 2019;8:7728–7740. [PubMed: 31642612]
45. Li WD, Zhou DM, Sun LL, et al. LncRNA WTAPP1 promotes migration and angiogenesis of endothelial progenitor cells via MMP1 through microRNA 3120 and Akt/PI3K/autophagy pathways. Stem Cells. 2018;36:1863–1874. [PubMed: 30171660]
46. Liu D, Zhang Y, Li X, et al. eIF2α signaling regulates ischemic osteonecrosis through endoplasmic reticulum stress. Sci Rep. 2017;7:5062. [PubMed: 28698612]
47. Li J, Li X, Liu D, et al. eIF2α signaling regulates autophagy of osteoblasts and the development of osteoclasts in OVX mice. Cell Death Dis. 2019;10:921. [PubMed: 31801950]
48. Kusumbe AP, Ramasamy SK, Starsichova A, et al. Sample preparation for high-resolution 3D confocal imaging of mouse skeletal tissue. Nat Protoc. 2015;10:1904–1914. [PubMed: 26513669]
49. Sundh D, Nilsson M, Zoulakis M, et al. High-impact mechanical loading increases bone material strength in postmenopausal women-a 3-month intervention study. J Bone Miner Res. 2018;33:1242–1251. [PubMed: 29578618]
50. Hatori K, Camargos GV, Chatterjee M, et al. Single and combined effect of high-frequency loading and bisphosphonate treatment on the bone micro-architecture of ovariectomized rats. Osteoporos Int. 2015;26:303–313. [PubMed: 25236876]
51. Wei FY, Chow SK, Leung KS, et al. Low-magnitude high-frequency vibration enhanced mesenchymal stem cell recruitment in osteoporotic fracture healing through the SDF-1/CXCR4 pathway. Eur Cell Mater. 2016;31:341–354. [PubMed: 27215741]
52. Tian GE, Zhou JT, Liu XJ, et al. Mechanoresponse of stem cells for vascular repair. World J Stem Cells. 2019;11:1104–1114. [PubMed: 31875871]
53. Liu X, Li Q, Niu X, et al. Exosomes secreted from human-induced pluripotent stem cell-derived mesenchymal stem cells prevent osteonecrosis of the femoral head by promoting angiogenesis. Int J Biol Sci. 2017;13:232–244. [PubMed: 28255275]
54. Xie Y, Chen Y, Zhang L, et al. The roles of bone-derived exosomes and exosomal microRNAs in regulating bone remodelling. J Cell Mol Med. 2017;21:1033–1041. [PubMed: 27878944]
55. Van Mil A, Grundmann S, Goumans MJ, et al. MicroRNA-214 inhibits angiogenesis by targeting Quaking and reducing angiogenic growth factor release. Cardiovasc Res. 2012;93:655–665. [PubMed: 22227154]
56. Huang J, Yin H, Rao SS, et al. Harmine enhances type H vessel formation and prevents bone loss in ovariectomized mice. Theranostics. 2018;8:2435–2446. [PubMed: 29721090]
57. Ji G, Xu R, Niu Y, et al. Vascular endothelial growth factor pathway promotes osseointegration and $CD31^{hi}EMCN^{hi}$ endothelium expansion in a mouse tibial implant model: an animal study. Bone Joint J. 2019;101-B:108–114. [PubMed: 31256654]

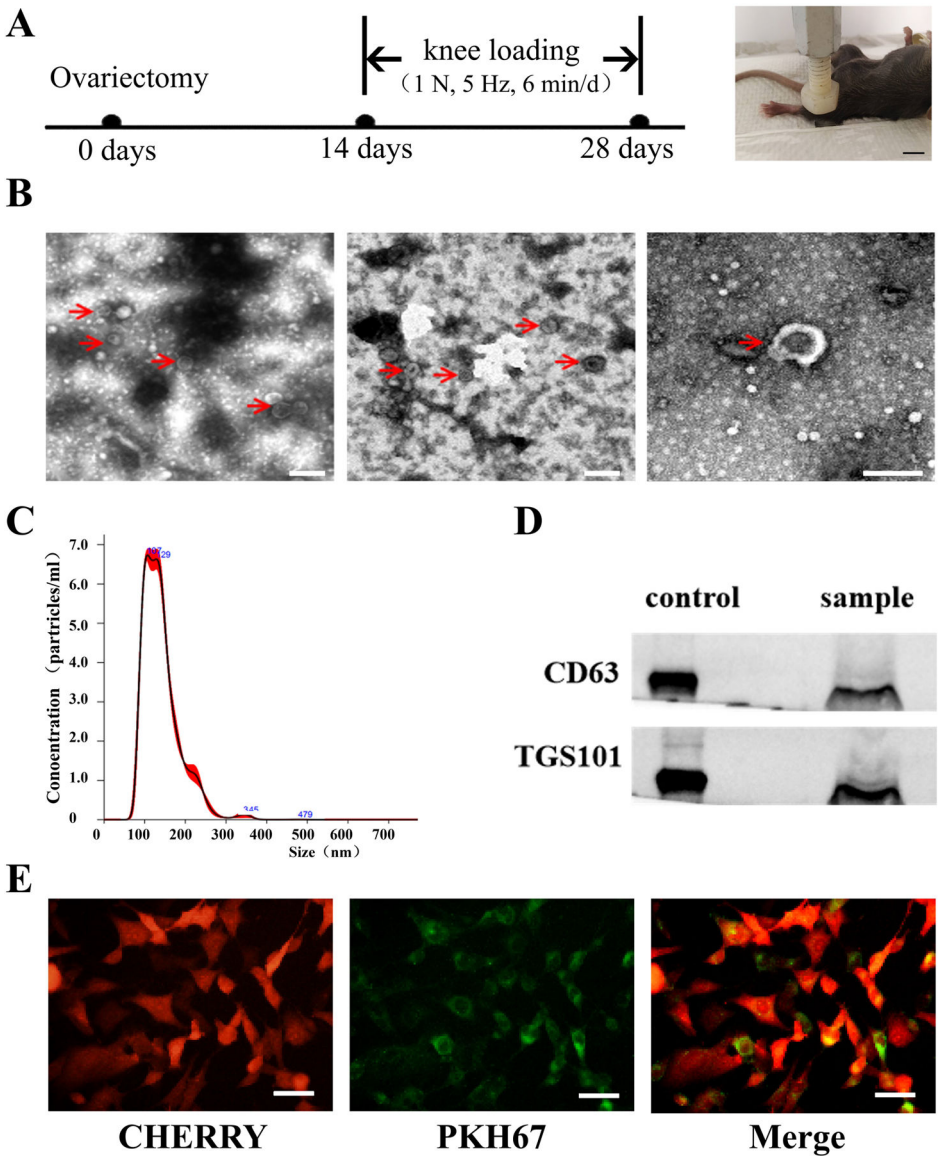

FIGURE 1.

Experimental setup, and the characterization of exosomes. A, Timeline (left) and loading site for knee loading (right, Bar = 1 cm). B, Morphology of exosomes with transmission electron microscopy, red arrows pointed to exosomes, Bar = 200 nm. C, The particle distribution was measured via nanoparticle tracking analysis. D, Protein markers of exosomes were detected by Western blot analysis. E, Representative images of HUVECs (red) incubated with PKH67-labelled exosomes (green) for 4 h. Bar = 50 μm.

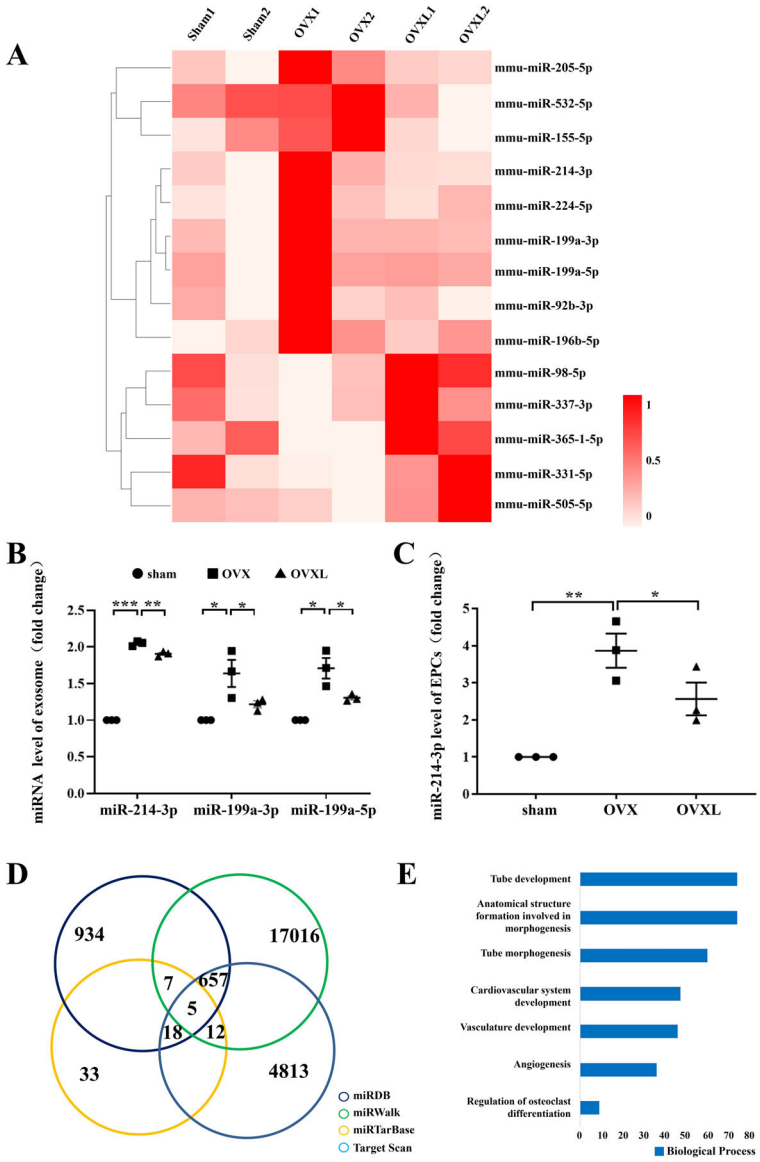

FIGURE 2.

Heat map and bioinformatics analysis of miR-214–3p. A, Heat map of differentially expressed miRNAs. The shade of red indicates the level of expression. B, miRNA expression in BMMSC-exosome. C, miR-214–3p expression in EPCs. n = 3 per group. **P* < .05, ***P* < .01 and ****P* < .001. D, Venn diagram of miR-214–3p target genes. The number indicates the predicted target genes. E, GO analysis of target genes for miR-214–3p.

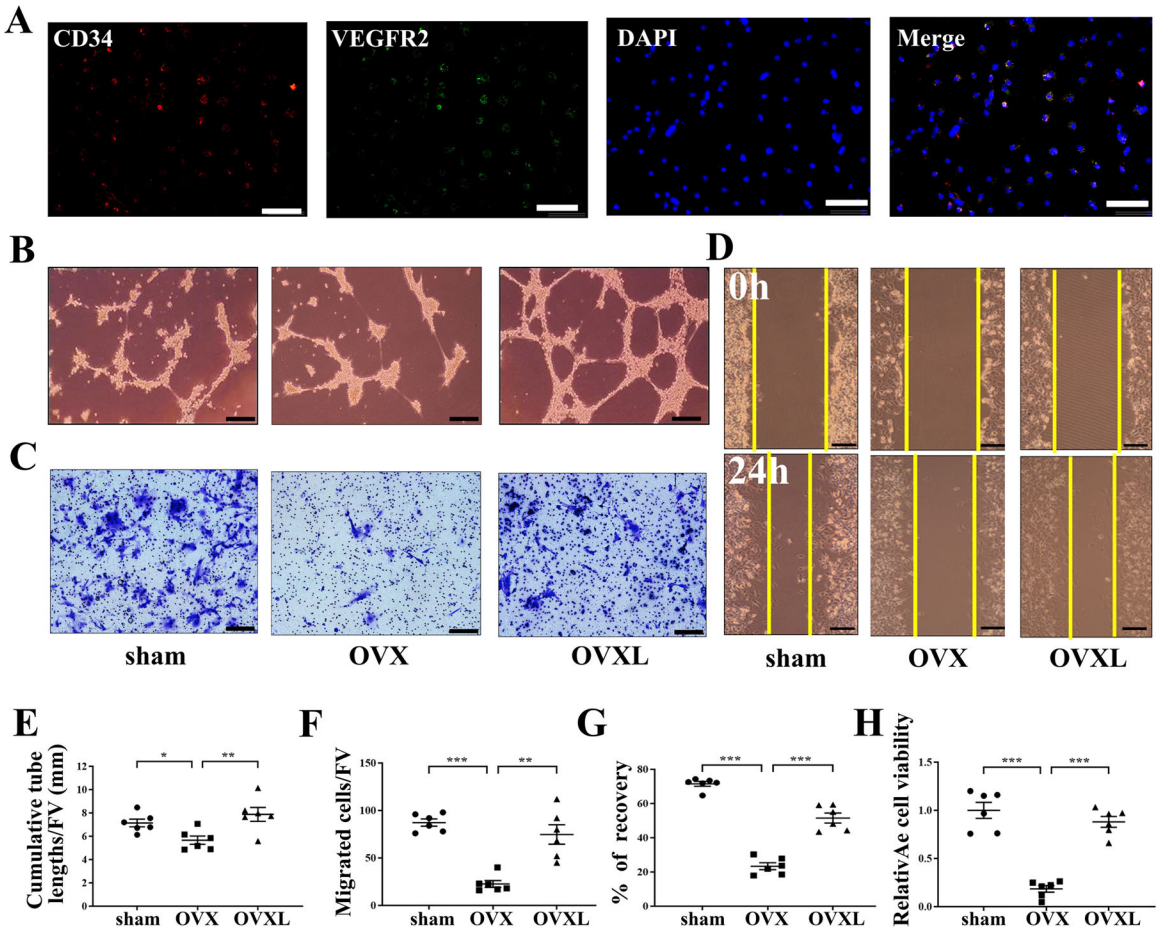

FIGURE 3.

Effect of endothelial progenitor tube formation, cells migration, and wound healing with knee loading in OVX mice *in vitro*. A, Double immunofluorescence staining of CD34 (red), VEGFR2 (green), DAPI cell nuclei (blue), and CD34, VEGFR2 together with DAPI (merge) on the same cell. Bar = 100 μm. B, Representative images of EPCs tube formation. Bar = 100 μm. C, Representative images of EPCs migration by crystal violet staining. Bar = 200 μm. D, Representative images of EPCs wound healing. Bar = 200 μm. E, Quantitative analysis of cumulative tube lengths. F, Quantitative analysis of EPCs migratory. G, Quantitative analysis of recovery. H, Relative cell viability was evaluated by MTT assay, Quantitative analysis of relative cell viability. Of note, FV, a field of vision. n = 6 per group. $*P < .05$, $**P < .01$ and $***P < .001$.

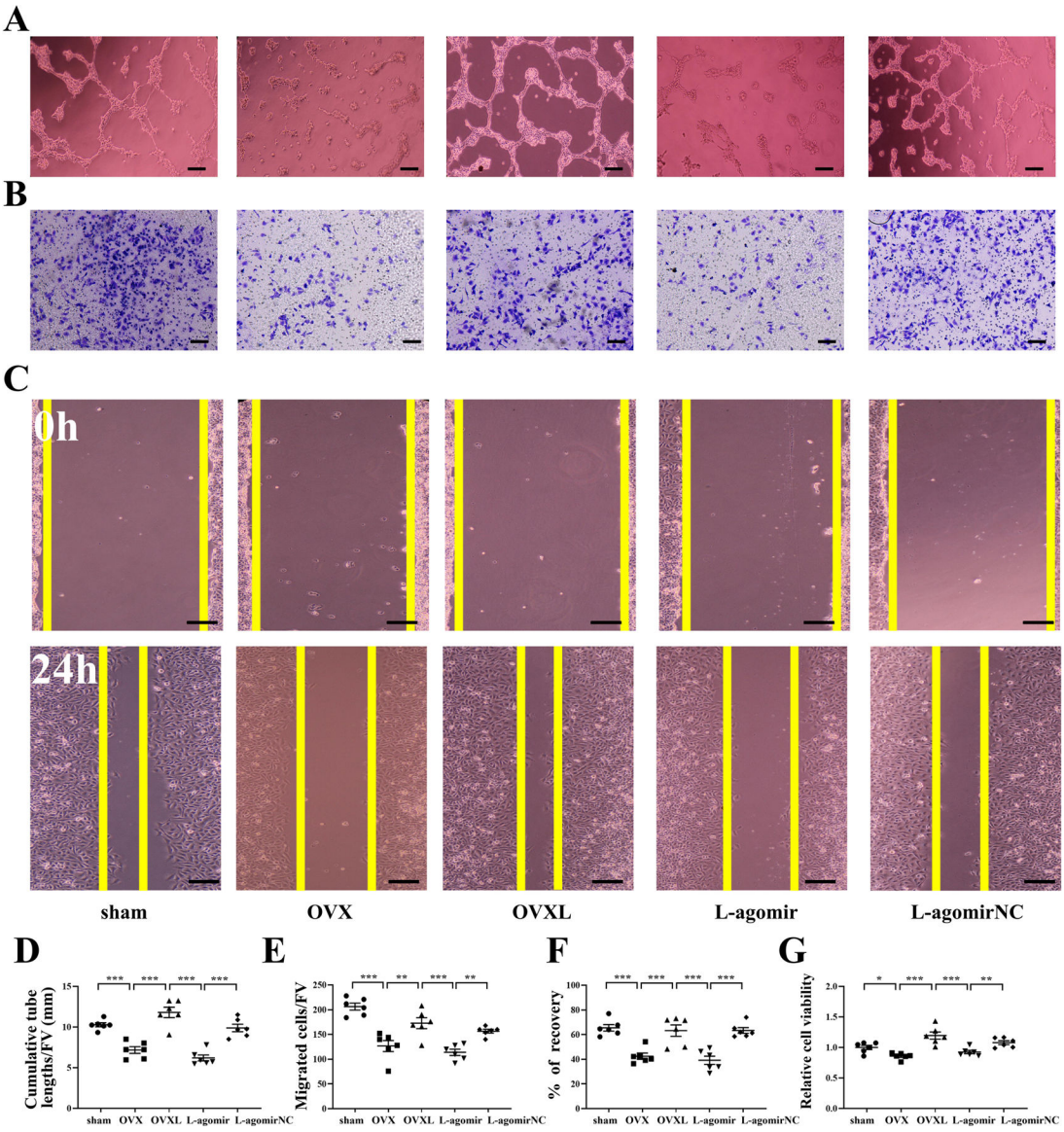

FIGURE 4.

Effect of BMMSC-Exos on tube formation, cell migration, and wound healing of HUVECs. A, Representative images of tube formation. Bar = 100 μm. B, Representative images of migration by crystal violet staining. Bar = 200 μm. C, Representative images of wound healing. Bar = 200 μm. D, Quantitative analysis of cumulative tube lengths. E, Quantitative analysis of migratory. F, Quantitative analysis of recovery. G, Relative cell viability was evaluated by MTT assay, Quantitative analysis of relative cell viability. Of note, FV, field of vision. n = 6 per group. **P* < .05, ***P* < .01 and ****P* < .001.

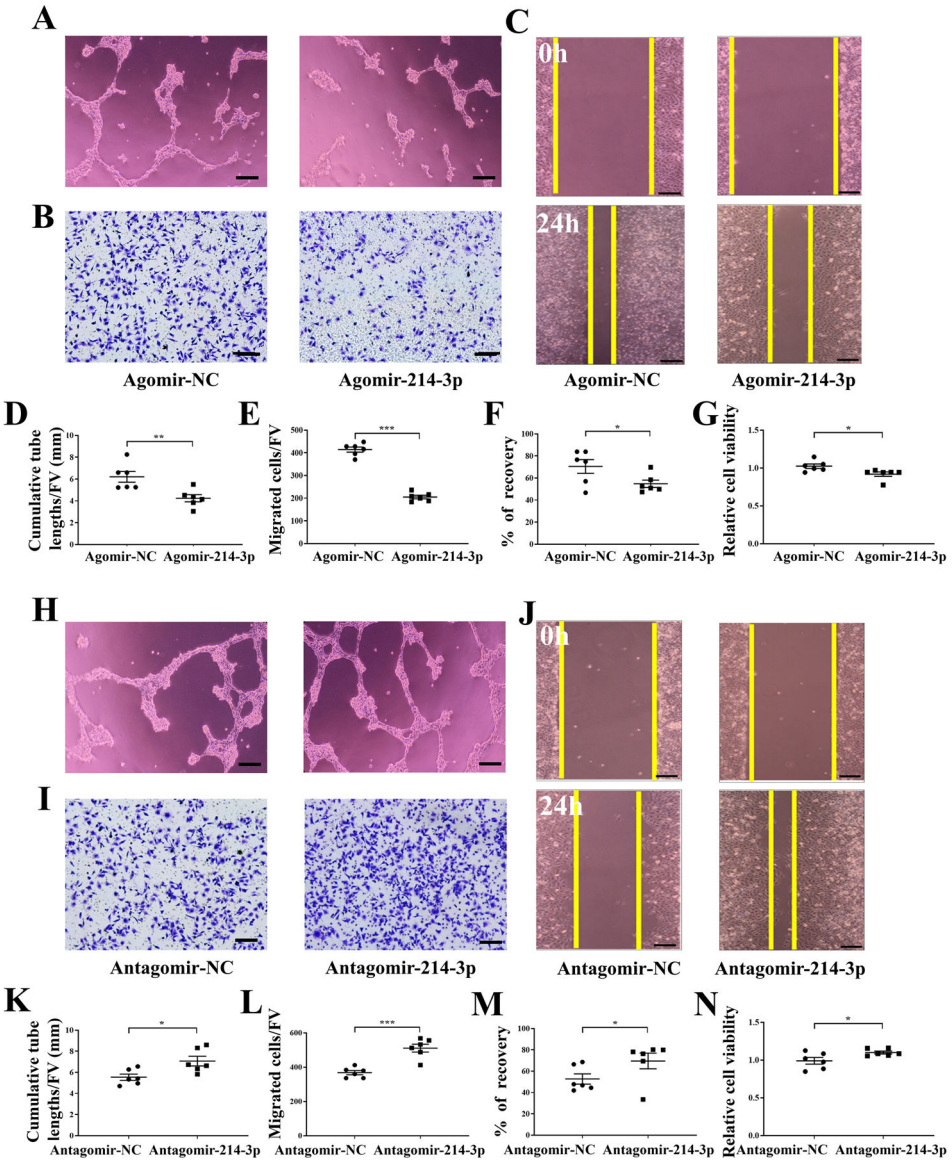

FIGURE 5.

Effect of miR-214–3p on HUVECs tube formation, migration, and wound healing. A, Agomir-214–3p decreased HUVECs tube formation in the matrigel system in vitro. Bar = 100 μm. B, Agomir-214–3p decreased HUVECs migration. Bar = 200 μm. C, Agomir-214–3p decreased HUVECs wound healing. Bar = 200 μm. D, Quantitative analysis of cumulative tube lengths. E, Quantitative analysis of EPCs migratory. F, Quantitative analysis of recovery. G, Statistical analysis for relative cell viability of HUVECs. H, Antgomir-214–3p increased HUVECs tube formation in the matrigel system in vitro. Bar = 100 μm. I, Antgomir-214–3p increased HUVECs migration. Bar = 200 μm. J, Antgomir-214–3p increased HUVECs wound healing. Bar = 200 μm. K, Quantitative analysis of cumulative tube lengths. L, Quantitative analysis of EPCs migratory. M, Quantitative analysis of recovery. N, Statistical analysis for relative cell viability of HUVECs. Of note, FV, field of vision. n = 6 per group. $*P < .05$, $**P < .01$ and $***P < .001$.

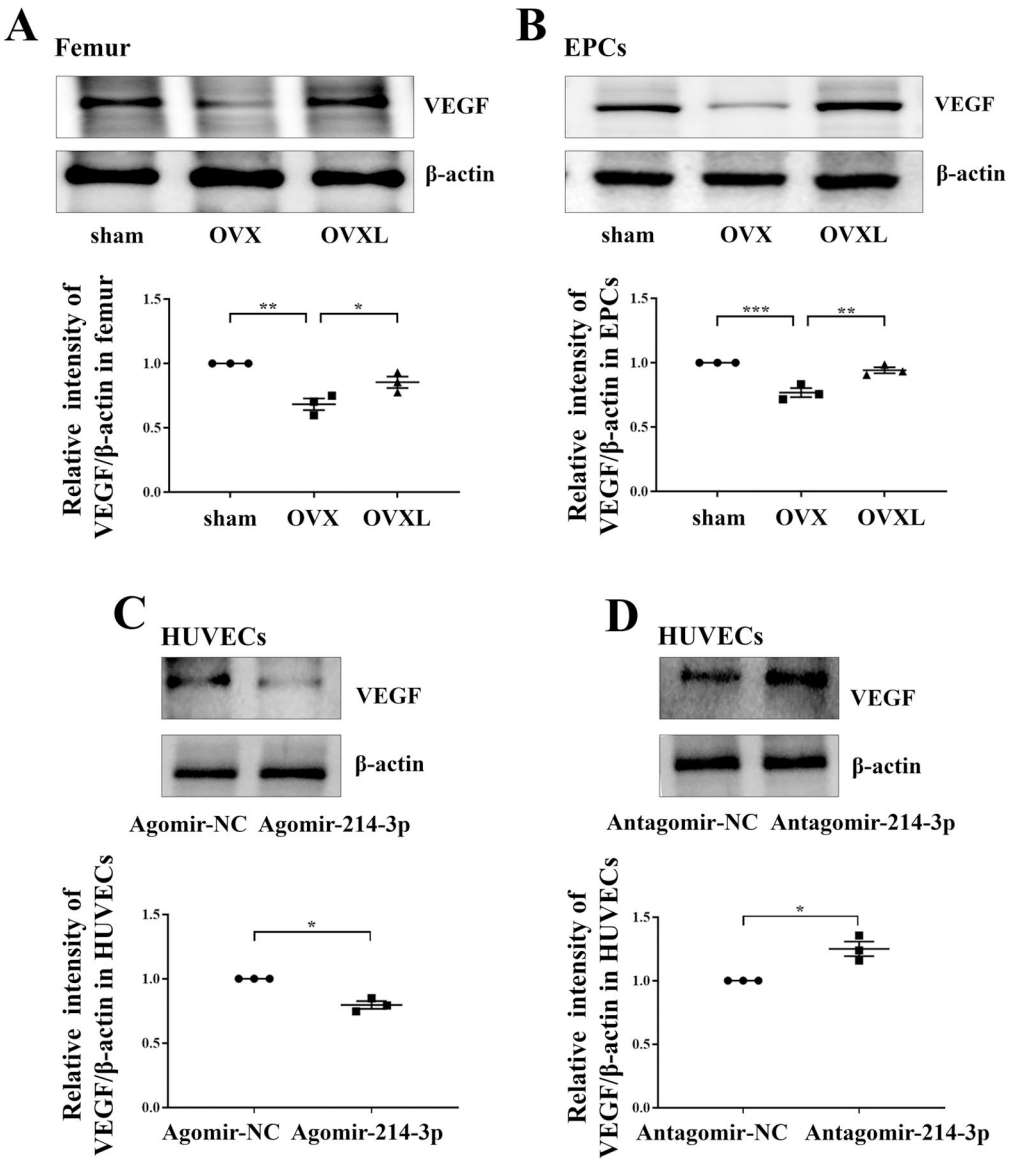

FIGURE 6.

MiR-214–3p-mediated promotion of bone angiogenesis by knee loading. A, Western blot showed the protein level of VEGF in the femur in OVX treated with knee loading. Representative images of Western blot of three different groups in vivo. Relative quantification of protein level of VEGF. B, Western blot showed the protein level of VEGF in EPCs in OVX treated with knee loading. Representative images of Western blot of three different groups in vivo. Relative quantification of protein level of VEGF. C, Western blot revealed that agomir-214–3p decreased the level of VEGF in HUVECs. Relative quantification of protein level of VEGF. D, Western blot revealed that antgomir-214–3p increased the level of VEGF in HUVECs. Relative quantification of protein level of VEGF. n = 3 per group. **P* < .05, ***P* < .01 and ****P* < .001.

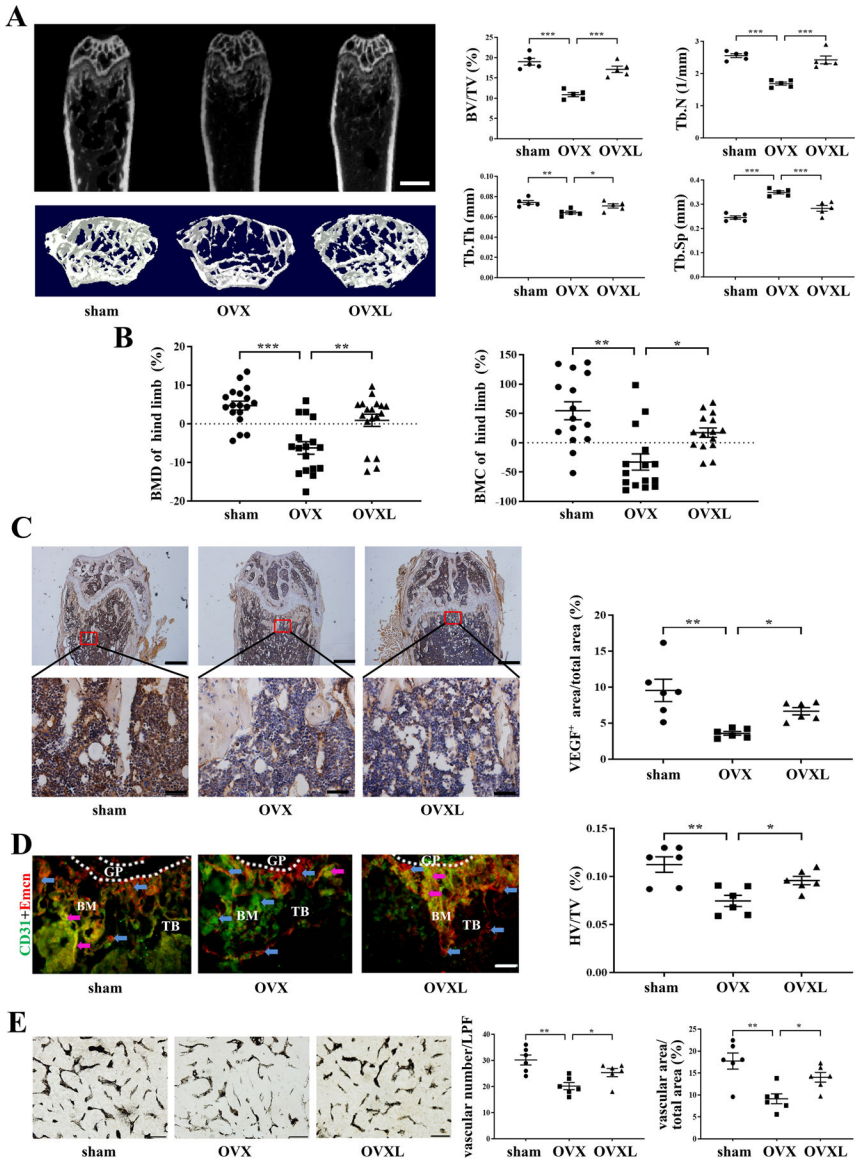

FIGURE 7.

Effects of ovariectomy and knee loading. A, Representative μCT images of the distal femur, scale bar = 1 mm. Quantitative analyses of bone volume/total volume (BV/TV), trabecular number (Tb.N), trabecular thickness (Tb.Th), and trabecular separation (Tb.Sp). n = 5 per group. B, Quantitative analyses of BMD and BMC of hind limb, n = 15 per group. C, The expression of VEGF was measured by immunohistochemistry assay. VEGF positive staining microvessels in distal femur were indicated by the red square. Upper bar = 500 μm, lower bar = 100 μm. The ratio of VEGF positively stained area to total field area was calculated. n = 6 per group. D, Immunofluorescence staining for $CD31^{hi}Emcn^{hi}$ vessel (type H vessel) formation. Type H vessels are a major connection between blood cells and bone formation. The frozen sections in the distal femoral metaphysis were stained with CD31 antibody (green), Emcn antibody (red). The red, green, and merged-color sections were taken as the total vessels. CD31 and Emcn merged region represents type H vessels (“H”, purple

arrowheads). The red and green areas represent non-H vessels (“non-H”, blue arrowheads). Bar = 100 μm. Quantitative analysis is the percentage of $CD31^{hi}Emcn^{hi}$ vessel (HV) numbers in total vessels (TV). n = 6 per group. E, Ink blood perfusion angiography was used to analyze the density of microvessels. Bar = 100 μm. Quantitative analysis of the vascular number and vascular area. n = 6 per group. Of note, BMD, bone mineral density; BMC, bone mineral content; BM, bone marrow; GP, growth plate; TB, trabecular bone; LPF, low power field. $*P < .05$, $**P < .01$ and $***P < .001$.

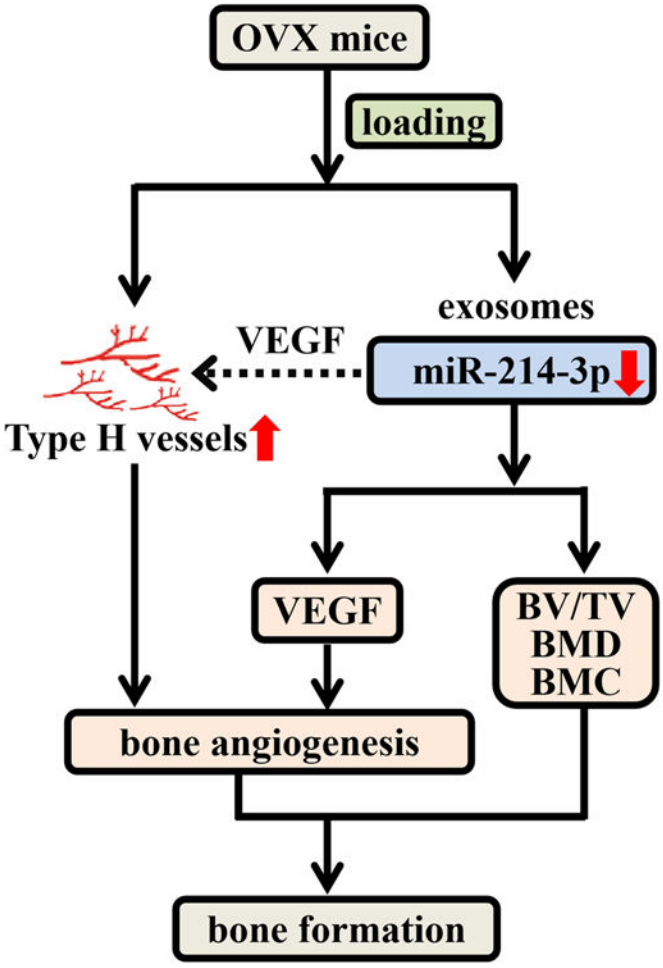

FIGURE 8.
Proposed mechanism of the formation of type H vessels and the role of miR-214–3p in the effect of mechanical loading on postmenopausal osteoporosis.

Table 1:

Primer sequences used for polymerase chain reactions.

Gene	Forward primer(5′−3′)	Reverse primer(5′−3′)
miR-214–3p	GCGACAGCAGGCACAGACA	AGTGCAGGGTCCGAGGTATT
U6	TCGGCAGCACATATACTAAAATTGGA	CGAATTTGCGTGTCATCCTTGC
VEGF	TAGAGTACATCTTCAAGCCGTC	CTTTCTTTGGTCTGCATTCACA
β-actin	GTGCTATGTTGCTCTAGACTTCG	ATGCCACAGGATTCCATACC

Note: VEGF: Vascular endothelial growth factor; miR-214–3p: microRNA-214–3p.